Applied Geochemistry 24 (2009) 16–31

Contents lists available at ScienceDirect

Applied Geochemistry

journal homepage: www.elsevier.com/locate/apgeochem

Salinization processes in the unconfined aquifer of Bou-Areg (NE Morocco): A geostatistical, geochemical, and tomographic study

F. El Yaouti [a,*], A. El Mandour [b], D. Khattach [a], J. Benavente [c], O. Kaufmann [d]

[a] Laboratory of LGA, Faculty of Sciences, University Mohammed I, Oriental Center of Water Science and Technology (COSTE), P.B. 524, Oujda, Morocco
[b] Laboratory of Hydrogeology, Faculty of Sciences Semlalia, University Cadi Ayyad, P.B. 2390, Marrakech, Morocco
[c] Water Research Institute, University of Granada, Ramon y Cajal, 4, 18071 Granada, Spain
[d] Polytechnic Faculty of Mons, Service of Fundamental and Applied Geology, Mons, Belgium

ARTICLE INFO

Article history:
Received 11 January 2008
Accepted 23 October 2008
Available online 5 November 2008

Editorial handling by R. Fuge

ABSTRACT

Hydrogeological and geochemical data, in conjunction with the results of an electrical imaging tomographic survey, were examined to determine the main factors and mechanisms controlling the groundwater chemistry and salinity of the unconfined aquifer of Bou-Areg, on the Mediterranean coast of NE Morocco. In addition, statistical and geochemical interpretation methods were used to identify the distribution of the salinity. Multivariate statistical analysis (cluster and principal component factors) revealed the main sources of contamination. Groups A, B, and C in the cluster analysis and Factors 1–3 (Factor 1: CE, Cl^-, K^+, SO_4^{2-}, and Mg^{2+}; Factor 2: Ca^{2+}, HCO_3^-, and pH; Factor 3: NO_3^-) represent the 'signature' of seawater intrusion in the coastal zone, the influence of marly-gypsum outcrops in the upstream zone, and anthropogenic sources, respectively. The ionic delta, the ionic ratio, the saturation index, and Stuyfzand's method were applied to evaluate geochemical processes. The results obtained indicate, on the one hand, the phenomenon of salinization in both the coastal and the upstream zones, and on the other, the dilution of groundwater by recharge. Cation exchange is shown to modify the concentration of ions in groundwater. Locally, with respect to salinization processes in the coastal zone, the results of electrical imaging tomography show that salinity increases both with depth and laterally inland from the coastline, due to seawater intrusion.

1. Introduction

Groundwater in coastal areas is vulnerable to salinization by seawater, which can make it unfit for drinking or agricultural use; moreover, groundwater salinization can be increased by natural processes and anthropogenic factors. The latter is a common phenomenon affecting Mediterranean groundwater (Capaccionia et al., 2005; Custodio, 1987; Dörfliger, 2003; El Baruni, 1995; El Mandour et al., 2006, 2008; Ferrara and Pappalardo, 2004; Grassi and Netti, 2000; Lambrakis et al., 1997; Petalas and Diamantis, 1999; Vincenzo and Giovanna, 2003). Generally, fresh groundwater that is not affected by pollution is characterized by low values of EC and Ca–Mg–HCO_3 water type. The latter represents freshwater that has recently infiltrated into the zone of recharge, while the EC shows a gradual increase from the uplands recharge areas towards the lowlands discharge areas. Along the coastline, high values of EC are usually attributed to salinization by seawater intrusion (Stamatis and Voudouris, 2003). However, there are cases where salinization is due to the presence of connate fossil waters (Worden et al., 2006). According to Appelo and Postma (1996), some water types characterise salt groundwater: Na–Cl dominant type, Ca–Cl, indicating the seawater intrusion process, and Na–Mg–Cl–SO4, representing a mixed water type. Water–rock interaction can alter groundwater; high-SO_4^{2-} concentrations can be associated with the dissolution of gypsum, which occurs in western Greece (Diamantopoulou, 1999). In addition, groundwater is affected by anthropogenic factors; NO_3^- pollution can be attributed to different sources, the most important of which are the uncontrolled application of fertilizers, untreated domestic effluent into abandoned wells, and the disposal of domestic and industrial wastewater.

Cation exchange is another factor modifying groundwater quality and is one of the most important geochemical processes taking place in aquifers. In coastal aquifers, where the relationship between seawater and fresh water is complex, cation exchange contributes significantly to the final composition of the groundwater. In detrital sedimentary aquifers, cation exchange is one of the most important geochemical processes of seawater intrusion (Cardona et al., 2004). The characteristic cation-exchange process that takes place when seawater intrudes a coastal fresh water aquifer (Appelo and Postma, 1996) is

* Corresponding author.
E-mail addresses: elyfouzia@yahoo.fr (F. El Yaouti), A.elmandour@ucam.ca.ma (A. El Mandour), dkhattach@yahoo.fr (D. Khattach), jbenaven@ugr.es (J. Benavente).

0883-2927/$ - see front matter © 2008 Elsevier Ltd. All rights reserved.
doi:10.1016/j.apgeochem.2008.10.005

$$2Na + (Ca_{1-x}Mg_x) - X \rightarrow (1-x)Ca + xMg + Na_2 - X(0 \leqslant x \geqslant 1) \quad (1)$$

where X indicates the exchanging solid surface.

The reverse process takes place with freshening, i.e., when fresh water intrudes a salt water aquifer:

$$(1-x)Ca + xMg + Na_2 - X \rightarrow (Ca_{1-x}Mg_x) - X + 2Na(0 \leqslant x \leqslant 1) \quad (2)$$

The freshwater resources of the Bou-Areg plain, located on the Mediterranean coast of NE Morocco (Fig. 1), are mainly composed of groundwater and the Selouane River. The groundwater is affected by the above-described phenomenon of salinization (El Mandour et al., 2006, 2007) and the Selouane River, which crosses the central plain of Bou-Areg and ends in the Bou-Areg lagoon, is characterized by very high salinity, with an average electrical conductivity of 9060 μS/cm in December 2006. The study area is bordered in the lowlands by the lagoon of Nador; the water of this lagoon is very saline, with an average salt content that has ranged between 37 g/L and 42 g/L over the last 30 a (Dakki et al., 2000). The study area has long been used for agriculture, and both river water and groundwater are exploited for irrigation. However, since the groundwater is severely affected by salinization, most water extracted for agriculture depends on the river water irrigation system. Nevertheless, the groundwater salinization may have been caused by natural processes rather then excessive pumping. Other important factors such as cation exchange and agricultural fertilizers, however, should also be considered. The population of the region has increased significantly, following remarkable economic development in sectors such as agro-food, textiles, chemistry, parachemistry, and steel (the last being based upon nearby iron mines in Sghanghan and Ouksan). In addition, various projects related to aquaculture (fish, oysters, shrimp, clams) have been set up in the Nador lagoon since 1982. Taking into account this economic development and demographic extension, a study of the groundwater quality is essential for future management and to prevent the deterioration.

Different methods have been used to study groundwater salinization and pollution. The evaluation of seawater intrusion has been dealt with through different approaches. Some authors (i.e., Hidalgo and Gruz-Sanjuhan, 2001; Jalali, 2007) have employed only geochemical methods based on variations of salinity and cation and anion concentrations, while others have introduced both geophysical and geochemical approaches to obtain a more comprehensive picture of this phenomenon (Cimino et al., 2008; Lee et al., 2001). Other authors have used multivariate statistical techniques, such as factor analysis (FA) and cluster analysis (CA) (i.e., Liu et al., 2003; Kim et al., 2003), to discuss geochemical evolution, mineralization, and groundwater contamination.

A research project was undertaken with the objectives of determining the hydrodynamic behavior of the groundwater and identifying and evaluating the main factors affecting groundwater quality. To accomplish these goals, statistical methods were used to classify and characterize groundwater quality. Stuyfzand's method, ionic ratios, ionic deltas, saturation indexes, and other geochemical methods of analysis were used to evaluate the sources of salinization. In order to test the reliability of the electrical imaging tomography method to characterize subsurface geological formations and to detect possible saline water intrusion, geophysical surveys were carried out in an area for which lithological borehole data were already available.

2. Geological and hydrogeological setting

The coastal plain of Bou-Areg covers a surface area of 190 km^2 (Fig. 1), bounded to the NW and W by the Gourougou and Ibn-Bou-Ifrour massifs and to the E by the Kebdana range. The northern part of the plain coincides with the arched shape of the Bou-Areg lagoon, also termed the Nador lagoon. To the S, it is bounded by the Selouane passage that connects it to the Gareb plain. The climate of the region is semi-arid, typically Mediterranean, with irregular annual rainfall; the average annual precipitation is around 346 mm.

North-Eastern Morocco, which includes the Bou-Areg basin, experienced the most recent marine transgression during the lower Pliocene. This transgression is characterized by marly deposits. After the retreat of the sea in the Villafranchien period, an extensive tectonic regime dominated by strong E–W extension (Morel, 1989) caused subsidence of the Bou-Areg basin. Thus, a lagunolacustrine regime and continental sedimentation characterizes

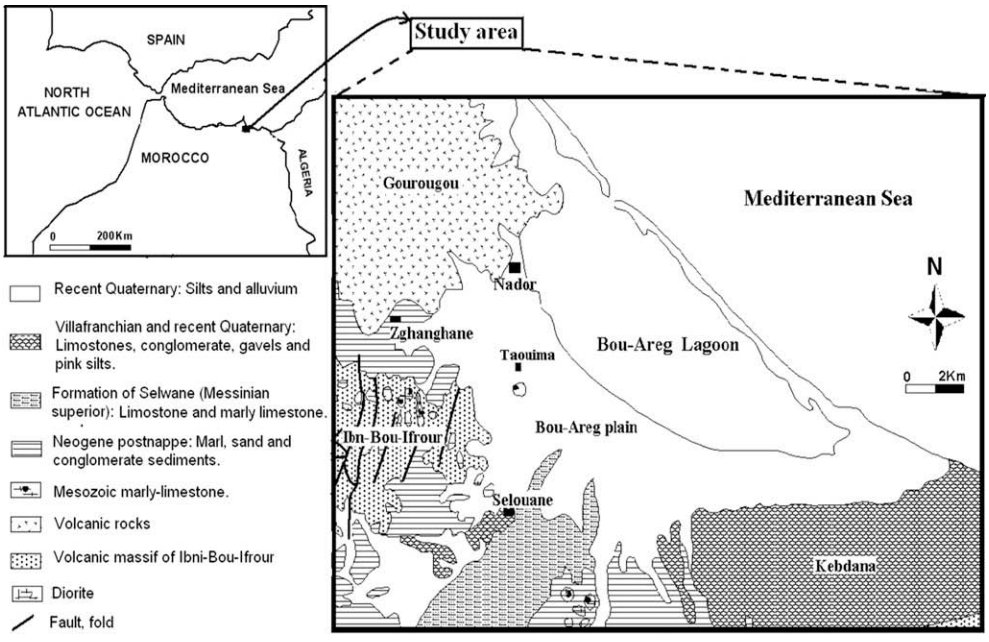

Fig. 1. Location map and geologic framework of the coastal Bou-Areg plain of Morocco.

the region. The sedimentation exceeded a depth of 80 m, and consists of clay, marls, silts, lacustrine limestone, and is associated with coarse elements of varied lithologies. Given that the Quaternary deposits were accompanied by tectonics, the sedimentation has been disturbed in this zone. In fact, some 30 boreholes have been drilled, revealing various sedimentary features, including layers and lenses. In terms of hydrogeological properties, these deposits are characterized by different degrees of permeability, in accordance with the grain size. It is possible to distinguish three principal formations. Formation 1 forms the upper layer, made up of fine materials with low permeability, including silts, clayey silts, encrusted limestones and marly-calcareous tufa that may contain gravels. Formation 2 is the bottom of the aquifer reservoir, grouping coarser elements with high permeability, such as pebbles, gravels of volcanic or sedimentary origin, and sands. Formation 3, which is reached by some boreholes, contains gypsiferous marls of Pliocene age. This formation represents the impervious bed to the upper Quaternary aquifer, dipping towards the lagoon. Thus, the Plio-Quaternary formations of Bou-Areg basin form an unconfined aquifer limited on the bottom by the Pliocene substratum of gypsiferous marls.

The Selwane formation (Fig. 1), attributed to the upper Messinian, consists of marls and intercalations of marly-limestone. The series is completed by marly-limestone with occasional intercalations of lagoon sediments. The Bou-Areg depression forms part of the Melilla-Nador Basin, one of the Mediterranean areas affected during the Late Miocene by the rapid and dramatic palaeoenvironmental change known as the Messinian Salinity Crisis (Hsü et al., 1973). This event was characterized by the deposition of thick evaporite materials in both peripheral and deep basins. It started at about 5.96 Ma (Lourens et al., 1996; Krijgsman et al., 1999), as a result of the closure of marine gateways between the Atlantic and the Mediterranean (Benson et al., 1991). This episode explains the existence of gypsiferous marls in Formation 3.

The plain is surrounded by geological formations with various facies (El Mandour et al., 2007) (Fig. 1). The Gourougou massif, bordering the plain to the NE and reaching a height of 887 m a.s.l., is a strato-volcano formed by three types of volcanic eruptions: (1) calc-alkaline (potassic trend); (2) intermediate (shoshonites, trachytes, and latites); and (3) alkali (basalt–sodium trend) (Barathon, 1989; Gill et al., 2004; Hernandez and Bellon, 1985). These volcanic events took place between the Messinian and the Plio-Quaternary (Morel, 1985). Although the primary porosity of the volcanic rocks is very low, tectonic activity has resulted in secondary porosity (fissured igneous rocks), which gives rise to a significant increase in permeability. Therefore, the volcanic rocks provide a suitable context for recharging and storing groundwater, and a sufficient quantity of water is obtained from the Bou-Areg plain, especially the Sghanghan region to the south of Gourougou. South of the Gourougou massif, the plain is bordered by the Ibn-bou-Ifrour complex (699 m a.s.l.), which is mainly composed of Jurassic deposits (limestone, limestone–sandstone and marls) and Cretaceous deposits (schisto-sandstone and volcano-sedimentary rocks). All of these are covered by the Miocene molasses. Part of the massif is crossed by micro-granodiorite veins, associated with hydrothermal mineralization (El Bakkali, 1995), resulting in the presence of Fe ore (Jbel Ouchxane).

The eastern boundary is defined by the Kebdana heights (937 m a.s.l.), where the deposits consist of Jurassic formations (marls and marly-limestones, sandstone, limestone–sandstone, limestone and dolomite-limestone) overlain locally by Miocene formations (limestone and marls) (Bloundi, 2005). Towards the Bou-Areg plain, the Kebdana range (Fig. 1) is made up of Villafranchian and recent Quaternary rocks (limestone, conglomerates, gravels, and silts). The Neogene post-nappe unit (Fig. 1) is comprised of marls, beds of sand and conglomerate levels.

Generally, the aquifer has good hydrodynamic characteristics (El Mandour et al., 2006, 2007). The highest permeability values, reaching 7×10^{-4} m/s, are found in the vicinity of the lagoon and in the western zone. Lower values are found at the borders of the Kebdana massif. Transmissivity varies continuously from upstream to the coastal zone, ranging from 9×10^{-4} to 2×10^{-2} m^2/s. The highest values are found in the west (north of the plain), whereas the lowest are measured at the borders of the Kebdana massif, probably due to the accumulation of marls. All along the coast, the transmissivity varies around 2×10^{-2} m^2/s. The potentiometric map obtained in December 2006 (Fig. 2) shows a general SW–NE groundwater flow, toward the lagoon, which forms the main outlet

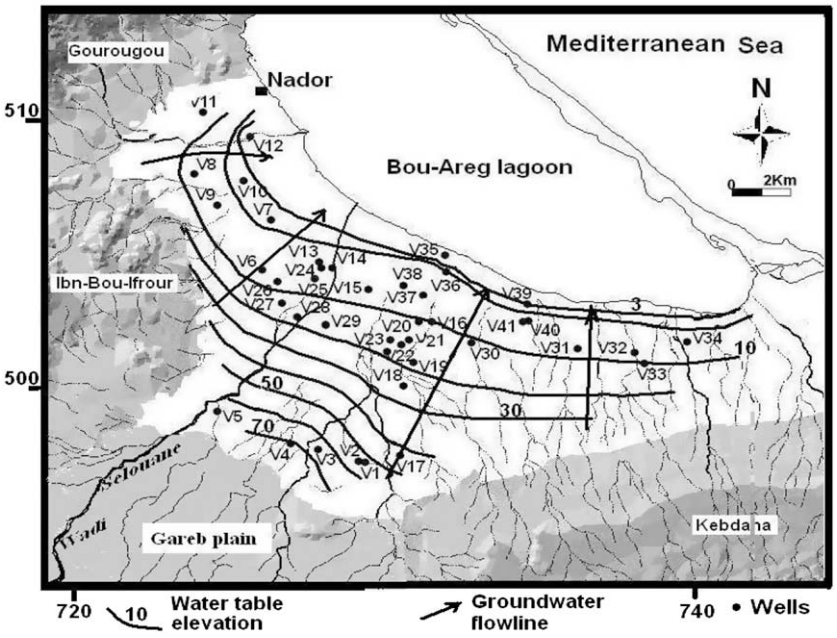

Fig. 2. Potentiometric map of the Bou-Areg unconfined aquifer (December 2006).

of the aquifer. Except for the upstream part of the aquifer, the hydraulic gradients are generally low (2–5‰).

3. Materials and methods

3.1. Sampling and analysis

Hydrogeological information was gathered from a sampling network set up in December 2006. As access to the wells is not entirely allowed by the population due to rite and private customs, only 41 wells were sampled. A sample of sea water was also analyzed.

The temperature, pH, and electrical conductivity (EC) were measured in the field. Chemical analyses of Na^+, Mg^{2+}, HCO_3^-, Cl^-, SO_4^{2-}, K^+ and NO_3^- were carried out in the laboratory of the Moulouya Water Basin Agency Oujda, using standard analytical procedures. Chloride, Ca^{2+}, CO_3^{2-}, HCO_3^- and Mg^{2+} were determined by titrimetric methods. Atomic absorption spectrophotometry was used to measure the concentrations of Na^+, K^+, NO_3^- and sO_4^{2-}. The quality of the chemical analyses was carefully inspected by checking ion balances. The chemical analyses were tested for charge balance error according to (Freeze and Cherry, 1979):

$$\%\text{Charge Balance Error} = \frac{\sum z \cdot m_c - \sum z \cdot m_a}{\sum z \cdot m_c + \sum z \cdot m_a} \cdot 100 \quad (3)$$

where z is the absolute value of the ionic valence, m_c is the molality of cationic species, and m_a is the molality of the anionic species.

Calculated charge balance errors are less than or equal to ±10%, which is an acceptable error for the purpose of this study.

3.2. Statistical analysis

Ten hydrochemical variables (including EC, Cl^-, Na^+, Mg^{2+}, HCO_3^-, SO_4^{2-}, K^+, Ca^{2+}, HCO_3^- and pH), and 41 samples were analyzed using multivariate statistical techniques. The values of the different variables (Table 1) were standardized prior to the multivariate analyses. The standardization step tends to minimize the influence of the difference of variance in variables, eliminates the influence of different units of measurement, and makes the data dimensionless (Liu et al., 2003). P variables were denoted $x_1, x_2 \ldots x_p$ in Table 1, each with N observations. The jth observation of the ith variable is $X_{i,j}$ and indicates the original value of the measured parameter, where $i = 1 \ldots P$ and $j = 1 \ldots N$.. The standardized value Z_{ij} is computed from the N observations of the ith variable and the mean and standard x_m and S_i, respectively:

$$Z_{ij} = \frac{X_{ij} - x_m}{S_i} \quad (4)$$

where the mean and variance of Z_{ij} are zero and one, respectively, for all values of i.

Hierarchical Cluster Analysis (HCA) and Principal Components Analysis (PCA) were used for the multivariate analysis.

HCA is a powerful tool for analyzing water chemistry data (Reeve et al., 1996). In this method, samples are grouped into dis-

Table 1
Physico-chemical results (ionic contents in mg/L) of the water sample analysis of Bou-Areg groundwater (December 2006), and depth of samples for each samples. EC: electrical conductivity (in μs/cm).

Wells	Depth of samples (m)	T (°C)	pH	CE	Cl	NO_3	HCO_3	SO_4	Na	K	Mg	Ca
V2	18.7	21.0	7.6	21000.0	7797.6	2.3	347.7	1473.9	3000.0	83.3	797.0	416.8
V3	18	21.0	7.4	9560.0	3039.1	12.5	390.4	576.3	1580.0	19.7	293.5	355.9
V4	7.9	21.7	7.3	9260.0	2779.1	44.9	463.6	805.8	1660.0	13.0	198.3	413.6
V5	12	21.5	7.6	13550.0	4318.7	68.8	408.7	1173.0	2080.0	18.0	337.8	248.5
V6	16	19.8	7.5	3400.0	529.8	20.1	524.6	616.1	840.0	9.7	63.2	32.1
V7	4.5	18.5	8.1	7620.0	1989.4	75.8	585.6	642.6	1480.0	28.0	116.6	121.8
V8	6	19.8	7.9	4900.0	899.7	31.7	725.9	814.0	1060.0	24.7	90.4	115.4
V9	12	20.3	7.8	4000.0	587.8	80.0	542.9	891.5	900.0	19.7	56.4	58.5
V10	4	4.8	7.9	5430.0	1055.7	89.9	542.9	948.6	1080.0	27.0	50.5	208.4
V11	20.2	22.1	7.5	4180.0	601.8	8.0	695.4	514.1	860.0	15.3	48.6	112.2
V12	8.7	19.8	7.6	3320.0	497.9	172.4	494.1	667.1	400.0	7.3	34.0	423.2
V13	6.2	21.4	8.1	2550.0	463.9	18.8	298.9	461.0	440.0	18.7	20.9	125.1
V14	8.3	18.4	7.7	8390.0	2539.2	32.3	359.9	856.8	1440.0	22.0	217.7	256.5
V15	10	20.5	7.4	6120.0	1624.5	28.9	469.7	561.0	1040.0	19.0	134.1	230.9
V16	11	19.7	8.0	5370.0	949.7	83.4	732.0	963.9	1300.0	17.3	46.7	102.6
V17	22.2	18.9	7.8	13140.0	4878.5	13.1	256.2	1387.2	2400.0	21.3	165.2	649.3
V18	22.8	18.2	8.2	3950.0	831.7	74.3	366.0	605.9	960.0	8.7	50.5	64.1
V19	17.5	20.2	8.3	4180.0	683.8	69.0	610.0	750.7	1100.0	11.3	22.4	41.7
V20	14.7	19.6	7.7	4910.0	969.7	49.2	585.6	969.0	1140.0	8.7	80.7	115.4
V21	6.2	20.5	8.2	3190.0	609.8	20.3	549.0	795.6	900.0	8.7	34.0	32.1
V23	15.4	20.2	8.0	4520.0	927.7	71.1	707.6	642.6	980.0	18.0	49.6	51.3
V24	5.4	19.3	8.0	6850.0	1879.4	40.5	457.5	770.1	1180.0	22.0	153.6	221.2
V25	12.4	20.3	7.6	7550.0	2179.3	43.3	366.0	260.1	1180.0	20.7	184.7	218.0
V26	15.3	20.7	8.0	6870.0	1749.5	55.5	732.0	1086.3	1420.0	18.0	83.6	70.5
V27	15	18.4	7.7	4640.0	891.7	133.4	854.0	567.1	960.0	19.3	25.3	160.3
V28	12.9	20.5	7.4	9650.0	3049.1	33.3	573.4	984.3	1480.0	18.0	200.2	304.6
V29	12.3	26.6	7.7	7370.0	2289.3	50.4	591.7	714.0	1260.0	18.7	155.5	243.7
V30	19.6	20.0	8.0	3630.0	507.8	18.2	768.6	750.7	700.0	23.0	93.3	89.8
V31	32.1	21.4	8.0	6200.0	1599.5	22.8	488.0	861.9	1200.0	17.3	116.6	96.2
V33	35	19.5	8.5	2610.0	445.9	25.1	579.5	605.9	740.0	11.3	30.1	48.1
V34	29	21.2	8.2	6210.0	1549.5	28.9	579.5	963.9	1360.0	17.7	75.8	51.3
V35	2.5	22.0	7.4	16080.0	5358.3	19.2	549.0	1086.3	2280.0	33.0	393.7	352.7
V36	3.6	20.5	8.1	5470.0	1199.6	45.8	610.0	943.5	1020.0	83.3	165.2	96.2
V37	6	18.0	8.3	5100.0	999.7	60.4	671.0	1076.1	1080.0	20.3	116.6	96.2
V38	4.5	20.8	7.8	6420.0	1639.5	31.2	677.1	1045.5	1220.0	83.3	165.2	125.1
V39	3.3	19.7	7.7	7080.0	1789.5	23.8	683.2	76.5	1160.0	250.0	165.2	144.3
V40	9.5	18.3	8.1	6170.0	1579.5	18.8	433.1	714.0	1220.0	27.3	153.6	131.5
V41	8.2	17.9	7.5	7730.0	2189.3	160.4	427.0	612.0	1260.0	29.0	210.0	246.9
Lagoon	–	16.2	8.3	53700.0	20993.5	9.9	170.8	3468.0	9800.0	368.0	1234.4	741.5

tinct populations according to their geological and hydrogeological contexts. The hierarchical (tree clustering) method is used to produce a graphical representation of individual groups using dendrograms. To perform CA, an agglomerative hierarchical clustering was developed using a combination of the Ward's linkage method (Word, 1963) and squared Euclidean distances as a measure of dissimilarity. To examine the chemical variation according to the groups, box plots (also called box-and-whisker plots) of individual variables are plotted. The line across the box represents the medium, whereas the bottom and top of the box show the locations of the first and third quartiles (Q1 and Q3), respectively. The whiskers are the lines that extend from the bottom and the top of the box to the lowest and highest observations inside the region defined by Q1 − 1.5 (Q3 − Q1) and Q3 + 1.5 (Q3 − Q1). Individual points with values outside these limits are plotted with asterisks.

PCA and Factor Analysis attempt by similar means to explain relationships between variables and thus infer the processes that control water chemistry (Helina et al., 2000). Factor analysis takes data contained in a correlation matrix and rearranges them in a manner that better explains the structure of the underlying system that produced the data. Therefore, the correlation coefficient matrix measures how well the variance of each constituent can be explained by relationships with each of the others. Then, the variances–co-variances and correlation coefficients of the variables are computed, and the correlation coefficient is

$$r_{X_{i,j},Y_{i,j}} = \frac{\sum(X_{i,j} - x_m)(Y_{i,j} - y_m)}{\sqrt{[(X_{i,j} - x_m)]^2[(Y_{i,j} - y_m)]^2}} \quad (5)$$

In this expression, the correlation coefficient ($r_{X_{i,j},Y_{i,j}}$) is simply the sum (over all samples) of the products of the deviations of the $X_{i,j}$-measurements and the $Y_{i,j}$-measurements on each sample, from the mean values x_m and y_m, respectively, for the complete set of samples. (Table 2) presents the matrix of correlation coefficients for the hydrochemical data in Bou-Areg. Eigenvalues and eigenvectors were calculated for the covariance matrix. Then the data were transformed into factors. (Table 3) presents the eigenvalues and the cumulative percentages of variance associated with each factor. Factor extraction was done with a minimum acceptable eigenvalue as 1 (Kaiser, 1958; Harman, 1960). Orthogonal rotation of these initial factors to terminal factor solutions (Table 2) was done with Kaiser's varimax scheme (Kaiser, 1958). Factor score coefficients are derived from the factor loadings. Factor scores are computed for each sample by a matrix multiplication of the factor score coefficient with the standardized data. The value of each factor score (Table 5) represents the importance of a given factor at the sample site. A factor score >+1 indicates intense influence by the process. Very negative values (<−1) reflect areas virtually unaffected by the process while near-zero scores reflect areas with only a moderate effect of the process. The spatial distribution of the factors (and hence the hydrochemical process represented by them) can be assessed by a contour of the factor scores representing each factor.

Table 3
Loading of the components obtained from principal component analysis, with two factors: Eigenvalue derived by factor analysis, and cumulative% explained by factors.

	F1	F2	F3
pH	0.007	0.761	0.057
CE	0.396	0.022	0.064
Cl^-	0.397	0.017	0.046
NO_3^-	−0.120	−0.145	0.942
HCO_3^-	−0.235	0.336	0.245
SO_4^{2-}	0.353	0.197	0.138
Na^+	0.389	0.116	0.086
K^+	0.310	0.234	0.065
Ca^{2+}	0.313	−0.421	0.106
Mg^{2+}	0.382	−0.040	−0.023
Eigen value	6.270	1.385	0.955
% Cumulative	62.700	76.546	86.094

Table 4
Hydrochemical classification (Stuyfzand, 1986).

Classification	Units	Limits	Code
Main type	Cl (mg/L)	<150	F: fresh
		150–300	Fb: fresh-brackish
		300–1000	B: brackish
		1000–10,000	Bs: brackish-salt
Type (total hardness)	Ca + Mg (meq/L)	0–½	*
		½–1	0
		1–2	1
		2–4	2
		4–8	3
		8–16	4
		16–32	5
		32–64	6
		64–128	7
		128–256	8
		> 256	9
Class $((Na^+ + K^+ + Mg^{2+})_{corrected} - \sqrt{(½Cl^-)})$	meq/L	0 (balance)	0
		>0 (excess)	+
Cation exchange situation		<0 (deficit)	−

* Very low.

3.3. Hydrochemical methods

Stuyfzand's method (1986) is used to identify the evolution of chemical processes in groundwater. The Stuyfzand's classification subdivides the most important chemical water characteristics at four levels: the main type, type, subtype, and class of a water sample. Each of the four levels of subdivision contributes to the total code (and name) of the water type.

The main type is determined based on the Cl^- content (in mg/L) (Table 4). The type is determined on the basis of an index for total hardness (TH) of the sample of water (Table 4); the total hardness is the sum of Ca and Mg (in meq/L) and is expressed by: TH (meq/

Table 2
Correlation matrix of 10 variables computed from chemical data for December 2006.

Variables	pH	CE	Cl^-	NO_3^-	HCO_3^-	SO_4^{2-}	Na^+	K^+	Ca^{2+}	Mg^{2+}
pH	1									
CE	0.017	1								
Cl^-	0.024	0.999	1							
NO_3^-	−0.051	−0.252	−0.264	1						
HCO_3^-	0.108	−0.518	−0.541	0.217	1					
SO_4^{2-}	0.239	0.888	0.886	−0.199	−0.382	1				
Na^+	0.125	0.984	0.983	−0.243	−0.482	0.910	1			
K^+	0.147	0.771	0.765	−0.234	−0.234	0.606	0.787	1		
Ca^{2+}	−0.355	0.751	0.761	−0.075	−0.627	0.612	0.690	0.450	1	
Mg^{2+}	−0.069	0.957	0.956	−0.300	−0.534	0.811	0.911	0.733	0.717	1

Table 5
Factor Scores and ionic ratios of chemical data (in meq/L) of Bou-Areg groundwater (December 2006).

Wells	Factor Scores			Ionic ratios						
	F1	F2	F3	Na^+/Cl^-	Ca^{2+}/Cl^-	Mg^{2+}/Cl^-	SO_4^{2-}/Cl^-	Na^+/Ca^{2+}	$(Ca^{2+} + Mg^{2+})/Na^+$	Ca^{2+}/SO_4^{2-}
V2	F1	F2	F3	0.59	0.09	0.30	0.14	6.27	0.66	0.68
V3	7.44	1.50	2.21	0.80	0.21	0.28	0.14	3.87	0.61	1.48
V4	0.23	7.28	3.70	0.92	0.26	0.21	0.21	3.50	0.51	1.23
V5	0.14	9.18	0.09	0.74	0.10	0.23	0.20	7.29	0.44	0.51
V6	0.71	2.13	0.49	2.44	0.11	0.35	0.86	22.83	0.19	0.12
V7	0.70	0.75	3.03	1.15	0.11	0.17	0.24	10.58	0.24	0.45
V8	0.17	0.85	1.21	1.82	0.23	0.29	0.67	8.00	0.29	0.34
V9	0.46	0.83	0.14	2.36	0.18	0.28	1.12	13.40	0.19	0.16
V10	0.57	0.06	0.98	1.58	0.35	0.14	0.66	4.52	0.31	0.53
V11	0.19	0.00	2.74	2.20	0.33	0.24	0.63	6.68	0.26	0.52
V12	0.81	0.15	2.82	1.24	1.50	0.20	0.99	0.82	1.38	1.52
V13	0.52	6.99	22.01	1.46	0.48	0.13	0.73	3.07	0.42	0.65
V14	0.46	0.00	4.92	0.87	0.18	0.25	0.25	4.89	0.49	0.72
V15	0.09	1.88	1.27	0.99	0.25	0.24	0.26	3.93	0.50	0.99
V16	0.08	3.93	1.65	2.11	0.19	0.14	0.75	11.04	0.16	0.25
V17	0.55	1.21	3.27	0.76	0.24	0.10	0.21	3.22	0.44	1.12
V18	2.57	4.91	1.60	1.78	0.14	0.18	0.54	13.04	0.18	0.25
V19	0.49	0.44	0.07	2.48	0.11	0.10	0.81	22.99	0.08	0.13
V20	0.80	3.59	0.63	1.81	0.21	0.24	0.74	8.61	0.25	0.29
V21	0.30	0.03	0.00	2.27	0.09	0.16	0.96	24.46	0.11	0.10
V23	0.63	3.63	1.80	1.63	0.10	0.16	0.51	16.64	0.16	0.19
V24	0.96	1.35	1.05	0.97	0.21	0.24	0.30	4.65	0.46	0.69
V25	0.01	0.00	0.33	0.83	0.18	0.25	0.09	4.72	0.51	2.01
V26	0.03	3.85	1.12	1.25	0.07	0.14	0.46	17.54	0.17	0.16
V27	0.25	2.80	0.62	1.66	0.32	0.08	0.47	5.22	0.24	0.68
V28	1.39	0.00	15.28	0.75	0.18	0.19	0.24	4.23	0.49	0.74
V29	0.07	2.37	0.20	0.85	0.19	0.20	0.23	4.51	0.46	0.82
V30	0.04	0.56	0.01	2.12	0.31	0.54	1.09	6.79	0.40	0.29
V31	0.78	2.50	0.76	1.16	0.11	0.21	0.40	10.87	0.28	0.27
V33	0.09	0.72	1.65	2.56	0.20	0.20	1.00	12.97	0.15	0.20
V34	0.91	7.21	1.17	1.35	0.06	0.14	0.46	23.10	0.15	0.13
V35	0.19	3.15	0.54	0.65	0.12	0.21	0.15	7	0.37	0.78
V36	1.25	2.83	0.67	1.31	0.14	0.40	0.58	9.24	0.41	0.24
V37	0.07	3.34	0.01	1.67	0.17	0.34	0.79	9.78	0.31	0.21
V38	0.30	4.82	0.71	1.15	0.13	0.29	0.47	8.50	0.37	0.29
V39	0.02	0.70	0.09	0.66	0.14	0.27	0.03	5.63	0.50	4.52
V40	0.00	0.49	0.57	1.19	0.15	0.28	0.33	8.09	0.36	0.44
V41	0.03	0.65	2.51	0.89	0.20	0.28	0.21	4.45	0.54	0.97
Lagoon	–	–	–	0.72	0.06	0.17	0.12	11.49	0.33	0.51

L) = ([Ca] + [Mg]) × 5; thus, the level attributed to this type depends on the total hardness value (Table 4). The classification into subtypes is determined based on the dominant cations and anions (in meq/L) in the triangle (Fig. 3). Finally, the class is determined on the basis of the sum of Na, K and Mg in meq/L, corrected for a sea salt contribution:

$$(Na + K + Mg)_{corrected} = (Na + K + Mg)_{measured} - 1.0716Cl \quad (6)$$

The factor 1.0716 is equal to [(Na + K + Mg)/Cl] in meq/L for mean ocean water. It is assumed that all the Cl ions are of marine origin (Eriksson, 1952). The value of the corrected sum values would be compared to the error margin $(0.5.\ Cl)^{1/2}$ depending on (table 4), which shows the method by which groundwater quality is classified. The deficit in the cation exchange represented by a negative sign results from salinization, and a positive sign indicates an excess in the cation exchange produced by the presence of fresh water; the cation exchange equilibrium shown by a zero describes a state of chemical balance.

The ionic ratio and the ionic delta are calculated in order to better understand the hydrochemical processes that take place in the aquifer. The ionic delta is derived from the relation between the actual concentration of each constituent and its theoretical concentration for a freshwater–seawater mix calculated for the Cl^- concentration of the sample. The saturation index (SI) of a mineral in solution is obtained using the method described by Appelo and Postma (1996), and is useful for evaluating the extent to which water chemistry is controlled by equilibrium with solid phases. PHREEQC software (Appelo and Postma, 1996) was used to calculate the SI for common evaporite minerals and the distribution of major aqueous species.

3.4. Electrical tomography

The concept of electrical imaging has been amply discussed in the geophysical literature (e.g., Loke and Barker, 1996; Tsourlos and Ogilvy, 1999; Zhang et al., 1995). Resistivity measurements are made for a large number of sets of four electrodes. Resistivity is determined by factors such as lithology, salinity of the pore fluid, water content, composition (mineral clay and metal content), porosity, grain size distribution and temperature (Berthold et al., 2004; Lashkaripour and Nakhaei, 2005; Löwner et al., 2005). Resistivity methods are routinely used to locate air filled voids. If the void is filled by water instead of air, its resistivity contrast with that of the host rocks may be quite small, and may even provide a resistivity low, depending on the salinity of the water.

For this study, the dipole–dipole electrode configuration illustrated in Fig. 4 was used and the apparent resistivity calculated by the formula shown.

The survey was conducted in the coastal zone of Bou-Areg (Fig. 5). Resistivity measurements were acquired along three profiles, termed L1, L2, and L3 (Fig. 5). For these profiles, the electrodes were oriented orthogonal to the coastline, and each had a total length of 475 m, with a maximum penetration depth of nearly 50 m. The data were collected using a multi-electrode Syscal-Pro

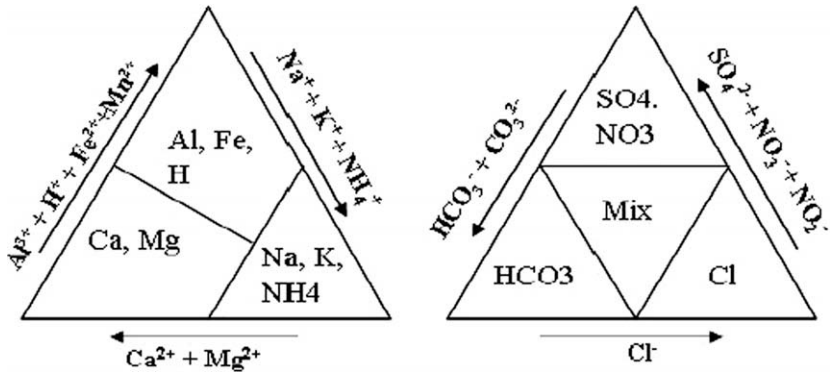

Fig. 3. Subdivision of types into subtypes on the basis of the proportional share of main constituents in the sum of the cations (left) and anions (right), both in meq/l.

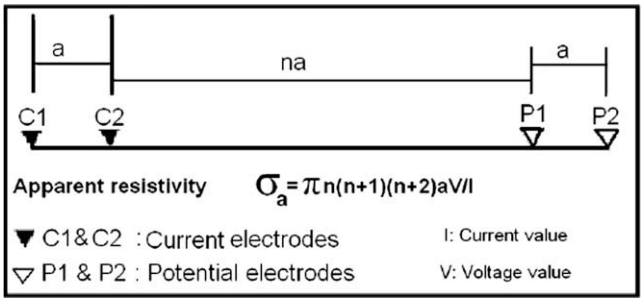

Fig. 4. Electrode configuration for the dipole–dipole array for resistivity surveys.

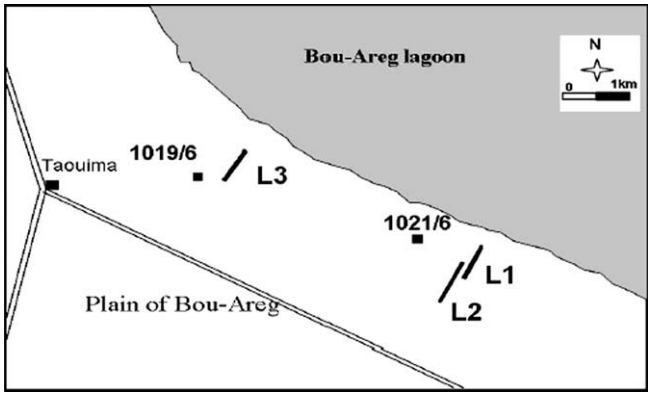

Fig. 5. Location of resistivity profiles L1, L2, and L3 and the location of boreholes 1019/6 and 1021/6.

system (IRIS Instruments), using 96 electrodes spaced at 5 m intervals. The measured apparent resistivity data were then inverted using RES2DINV software to create a resistivity model of the subsurface based on iterative smoothness-constrained least squares (Loke and Barker, 1996; Loke, 2002). This scheme requires no previous knowledge of the subsurface, the initial-guess model being constructed directly from field measurements.

4. Results and discussion

4.1. Hydrochemistry

(Table 1) shows the physical–chemical characteristics of the groundwater in the study area in December 2006. The temperature ranges from 18 to 26.6 °C, and pH ranges from 7.26 to 8.5, with an average of 7.25, thus indicating a slight tendency towards a basic composition. Electrical conductivity varies between 2210 and 21000 μS/cm, with an average of 6794 μS/cm; 82% of the samples gave values between 4000 and 21000 μS/cm, and 18% were between 2000 and 4000 μS/cm. This high salinity is determined by the predominance of the major ions Cl^- and Na^+, which correlate well with the electrical conductivity ($r = 0.99$ for Cl^- and 0.98 for Na^+ (Table 2).

Consequently, the waters are mostly classified as Na–Cl facies, borne out by the fact that the Na–Cl waters are mainly situated downstream, close to the lagoon and upstream from the plain. Other water types in the eastern and western zones of the plain contain a net enrichment in SO_4^{2-}, Ca and Mg.

4.2. Multivariate statistical analysis

4.2.1. Cluster analysis

Cluster Analysis was used to split the standardized physical–chemical data into groups of similar hydrochemical composition. (Fig. 6) shows the resulting dendrogram for the groundwater in the study area. The groundwater was classified into three main groups (A, B, C), according to their proximity to the coastline and the upstream zone of the plain. Group A is characterized by high salinity and is located in the upstream zone and downstream close to the coast. Groups B and C are characterized by medium salinity and are located in the western and eastern areas, respectively.

Individual variables were box-plotted to reveal the chemical variations between the groups. (Fig. 7) shows box plots for variables related to the groundwater quality, such as EC, Cl^-, Na^+, Mg^{2+}, HCO_3^-, SO_4^{2-}, K^+, Ca^{2+}, pH and NO_3^-. Differences between the groups are apparent; EC, Na^+, Cl^-, Mg^{2+}, Ca^{2+} and SO_4^{2-} have high concentration in group A and medium salinity in group C, which together contain most of the points in the aquifer. However, group B has a high concentration of NO_3^-, HCO_3^-, Ca^{2+} and pH.

About 8% of the samples in group B and 42% of those in group C have a higher NO_3^- concentration than Moroccan drinking water standards (40 mg/L), indicating that this group has been severely contaminated by nitrates (Fig. 6). As these wells are situated in the central zone, where agricultural activities are intense, and in the western zone, which is characterised by a high population density (the town of Nador), these nitrates are considered to be of anthropogenic origin, such as the leakage of domestic and industrial wastewater and the use of chemical fertilizers. An aggravating factor is that only Nador has a wastewater treatment plant, with an output rate of around 70% (Dakki et al., 2000; El Mandour et al., 2007), while other urban areas channel wastewater directly into the Selouane River, which crosses the Bou-Areg plain and flows into the lagoon.

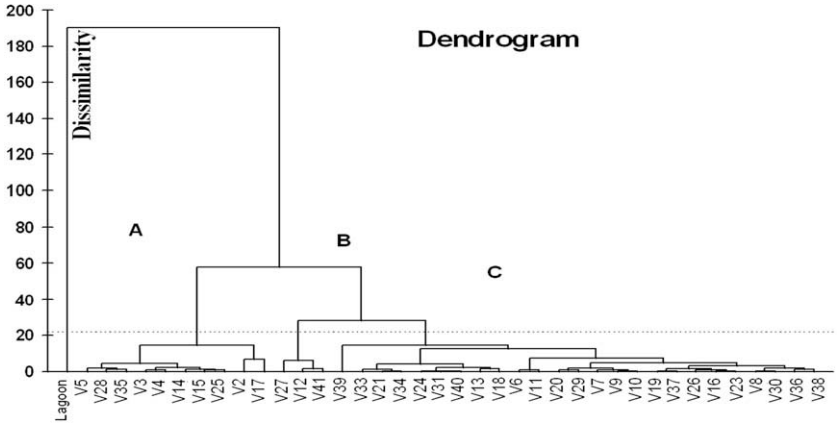

Fig. 6. Results of cluster analysis shown by a dendrogram (December 2006).

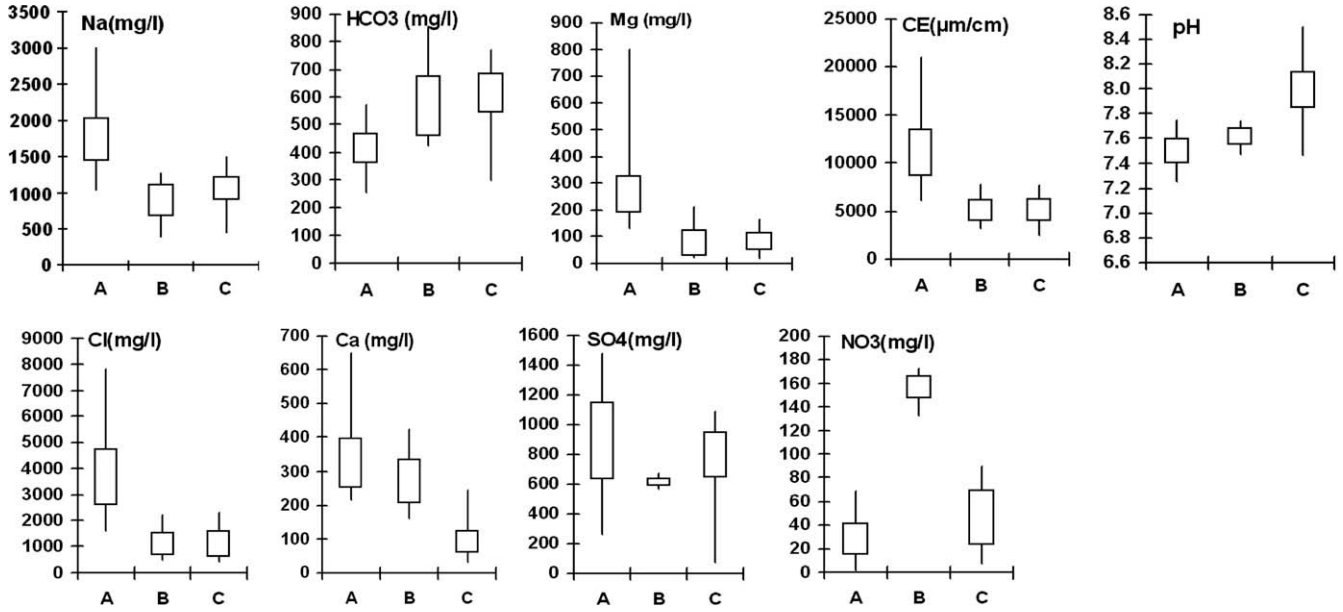

Fig. 7. Box plots of EC, Cl^-, Na^+, Mg^{2+}, HCO_3^-, SO_4^{2-}, Ca^{2+}, pH and NO_3^- for groundwater groups A, B and C (December 2006).

The groundwater in group A is mainly located in the upstream zone and downstream close to the lagoon (Fig. 6). This group has high salinity (EC, Cl^-, Na^+, Mg^{2+}, K^+ and SO_4^{2-}); this may be due to the seawater in the coastal area and to the influence of marly-gypsum outcrops in the upstream zone (more details on this will be discussed below). However, group C, located in the central, eastern and western zones, is characterized by low concentrations of these parameters.

4.2.2. Factor analysis

(Table 3) presents the eignvalues of the first 3 factors (F1, F2, and F3), their percentage of variance, and cumulative of variance. The eignvalues of the 3 factors, which exceeded one, explain 86.09% of the total variance. A factor score associated with each monitoring well was determined, and the scores are plotted to illustrate the spatial characteristics of groundwater quality of the Bou-Areg aquifer (Figs. 8–10).

Factor 1 has a high loading of EC, Cl^-, Na^+, Mg^{2+}, Ca^{2+}, K^+ and SO_4^{2-} and accounts for 62.7% of the total variance (Table 3). The hydrochemical items are the dominant solutes in seawater, especially Cl^- and Na^+ ($r = 0.98$ for raw data in Table 3), and in the region where the weathering of evaporites occurred. Therefore, factor 1 describes the salinization factor. The components of the salinization factor are similar to the 'seawater salinization factor' in Yun-Lin, Taiwan (Liu et al., 2003) and to 'processes of the evaporite dissolution rocks' in Alto Guadalentín, SE Spain (Ceron et al., 2000). The spatial distribution of the scores of factor 1 (Fig. 8) shows two areas with high values, one towards the upstream (V1, V3, V4) and the other towards the downstream (V35, V36, V37). These high scores could be due to seawater in the area close to the Bou-Areg lagoon. One zone in the upstream plain with high scores could be related to the influence of marly-gypsum outcrops in the upstream zone and to the processes of dissolution of the evaporite rocks (Messinian formation (Fig. 1) enriched in evaporate and gypsiferous materials), furthermore, the zone could be influenced by run-off and hence infiltration of superficial salty waters into the aquifer, which contribute significantly to the groundwater salinization.

Factor 2 explains 13.84% of the total variance (Table 3), with strong loadings of HCO_3^-, Ca^{2+} and pH, comparable with group C in the Cluster Analysis. This factor describes factor dilution of groundwater by water recharge and/or mineralization by water–

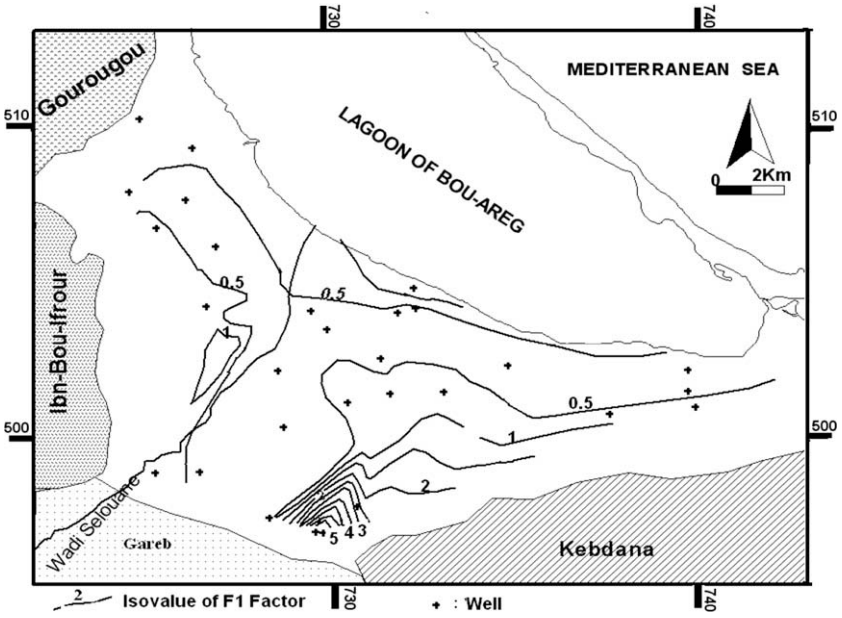

Fig. 8. Spatial distribution of F1 Factor scores (December 2006).

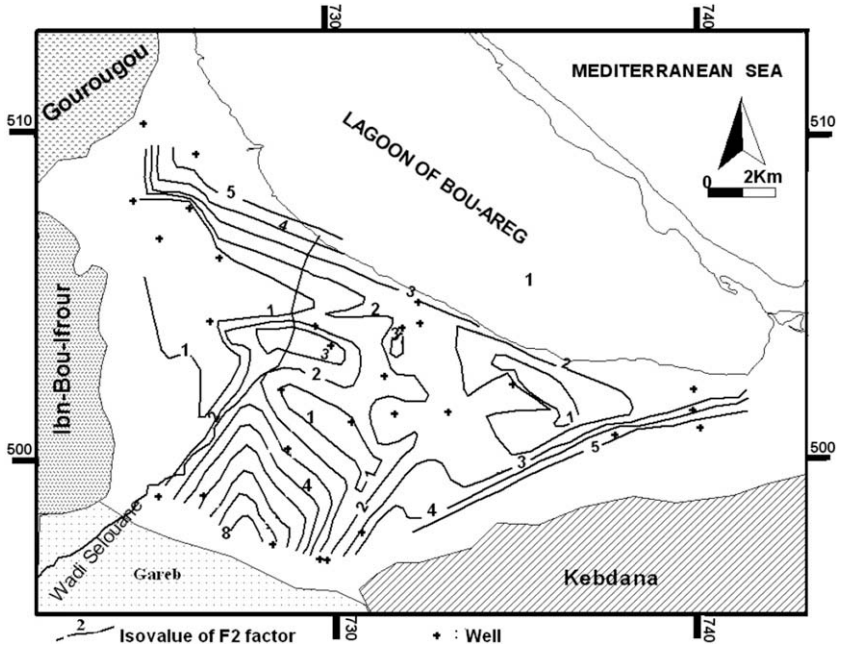

Fig. 9. Spatial distribution of F2 Factor scores (December 2006).

soil/rock interaction. The opposite evolution of Ca^{2+} and HCO_3^- in factor 2 indicates another source in addition to carbonate weathering, such as dissolution of gypsum and cation exchange that increases the Ca content. (Fig. 9), which shows the spatial distribution of factor 2, shows that high concentrations of Ca^{2+} and HCO_3^- occur in the zones bounding the aquifer (Ibn-Bou-Ifrour and Kebdana massifs). This excess may be related to the effect of the geological formations; the entry of fresh water due to rainfall into the aquifer dissolves carbonate rocks. Locally, in the central zone and urban zone of Nador, the high scores can be related to water infiltration from irrigation recharge and leakage of domestic waters into the aquifer during the sampling period. In addition, the presence of carbonate rocks such as calcite and dolomite in the sediments causes the high HCO_3^- concentrations throughout the aquifer, which range between 256.20 mg/L and 854 mg/L. This interpretation is corroborated by the secondary loadings of Ca^{2+} and HCO_3^- in Factor 3, as discussed below.

Factor 3 explains 9.55% of the total variance and is associated with groundwater with high concentrations of NO_3^-, and moderate concentrations of HCO_3^-, Ca^{2+} and SO_4^{2-}, such as group B in the cluster analysis. The NO_3^- pollution is serious in the Bou-Areg plain, and the NO_3^- concentrations in the monitoring wells exceed the standard of drinking water (40 mg/L.) because of extensive agricultural activities in the region, superficial N sources such as fertilizer, and domestic wastewaters, all of which significantly influence the groundwater quality through soil infiltration. The spatial

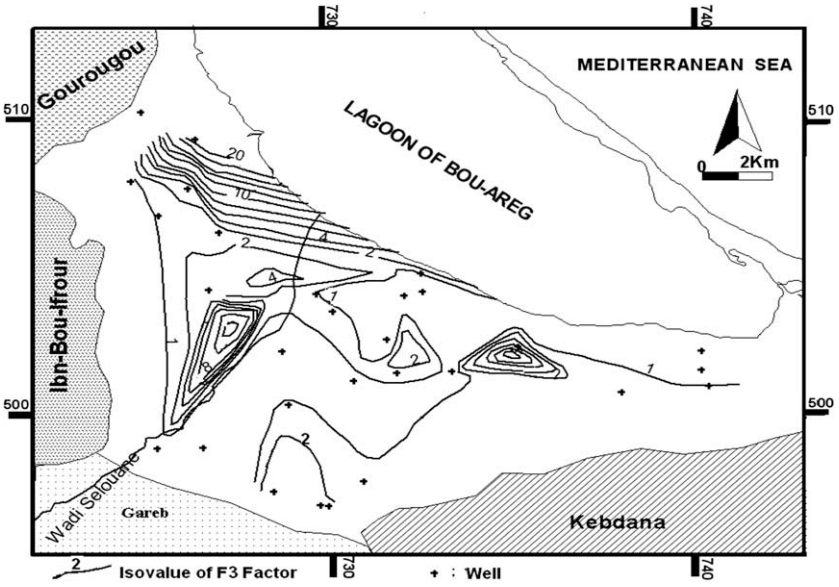

Fig. 10. Spatial distribution of F3 Factor scores (December 2006).

distribution of the factor scores of F3 (Fig. 10) shows 3 areas of high NO_3^- contamination. Two zones are in the central plain and one zone is in the urban region near Nador city. The potential sources of the NO_3^- pollution in the study area could be linked to wastewater leakage from industrial activities and urbanization. However, part of the NO_3^- contamination is from natural N in the soil, released to the unsaturated zone due to intense cultivation. Through nitrification processes by microbial oxidation in the presence of O_2, NH_4^+ is transformed into NO_3^- in the unsaturated zone (Stumm and Morgan, 1996) and can be described by the following equation: $NH_4^+ + 2O_2 = NO_3^- + 2H^+ + H_2O$. Association of high concentration of NO_3^- with low Ca^{2+} and SO_4^{2-} concentrations to factor 3 provides evidence for the use of fertilizers with SO_4^{2-}, Ca^{2+} and NH_4^+.

4.3. Geochemical processes

Based on Stuyfzand's classification (1986), the chemical groundwater types of the study area were distinguished and distributed spatially, as shown in Fig. 11. The results show three trends: in the upstream, central and downstream zones of the aquifer, the water types are mainly BS_4NaCl, BS_5NaCl, and BS_6NaCl, indicating that the waters are brackish and enriched with Cl^- and Na^+; the hardness of the water increases from 4 to 6 downgradient towards the Bou-Areg lagoon and upgradient towards the upstream zone. The water types in these two regions are negative, which explains that the salt waters intrude the groundwater. The salinization could be due to seawater intrusion in the zone close the lagoon, and it could also be linked to interactions between groundwater and marly substratum in the upstream zone. A positive sign of water types in the central zone indicates the dilution of groundwater with fresh water; the infiltration of irrigation water in this zone is thought to be the source of groundwater dilution. The eastern and western zones are also brackish, with the predominant water types in the eastern zone being B0Na–Cl–SO_4–HCO_3, B1Na–Cl–SO_4–HCO_3, B2Na–Cl–SO_4–HCO_3, and B3Na–Cl–SO_4–HCO_3. In the western zone, however, the water type changes from B4NaMix to B4CaMix towards the Gourougou massif. Somewhat less brackish water quality, with a positive sign, was identified in these areas, and may be explained by recharge from the Gourougou, Ibn-Bou-Ifrour, and Kebdana massifs, which refreshes the aquifer and restricts the mixing of fresh and salt water, consequently limiting the degree of salinization. This latter effect is assigned by the dominance of Cl^- rather than HCO_3^- ions in the salt water. The results of this method corroborate the results of the cluster and factor analysis.

The dominant groundwater type is NaCl, which explains that the waters are brackish in the study area. If the salt water intrudes the aquifer, the Na^+ is adsorbed on the clay fraction, and Ca^{2+} is released, and, consequently, the CaCl water type should be developed as according to Appelo and Postma (1996). However, in the study, the salinization phenomenon occurred in the upstream and downstream zones, but the CaCl water type has not been developed. This fact suggests that these zones are in the first state of salinization; the Stuyfzand's method indicates that the salinization phenomenon influences only the water type sign that is negative in the upstream and downstream zones; thus, the development of type NaCl to CaCl has not been achieved. Otherwise, the positive sign generalizes all waters types of Bou-Areg aquifer (Stuyfzand's classification) and supports the idea of groundwater dilution by infiltration of irrigation water and recharge from the massifs bounding the aquifer.

The chemical composition of the salts in the groundwater is slightly different from that of seawater, due to differences in the hydrochemical processes taking place, i.e., rock–water interaction in the former case and water recharge in the latter. In fact, the relationship between Cl^- and Na^+ (Fig. 12) shows that all samples plot above the fresh–seawater mixing line, except samples V2 and V35. This enrichment in Na^+ relative to Cl^-, with the Na^+/Cl^- ratio (Table 5) greater than the sample from the lagoon (0.72), and the corresponding depletion in Ca^{2+} and Mg^{2+} over Na^+ at some points, suggests a strong water–aquifer interaction related to dilution of halite and direct cation-exchange reactions between groundwater and the clay fraction of the aquifer material. This reaction takes place during the refreshening stage when freshwater flushes seawater in a coastal aquifer, displacing the freshwater/saltwater interface towards the lagoon. During refreshening, Na^+ is released to the groundwater because, where seawater saturates the aquifer, the Na/Ca ratio at the clay surface is higher than in the freshwater aquifer. The relationships between Cl^- and Na^+, and Ca^{2+} and Mg^{2+}, (Fig. 12) indicate that there are cases where samples (i.e., V17, V15, V36, V41, V3, V5, V28, V10, V12) plot above the fresh-seawater mixing line. This suggests other sources for the enrichment in

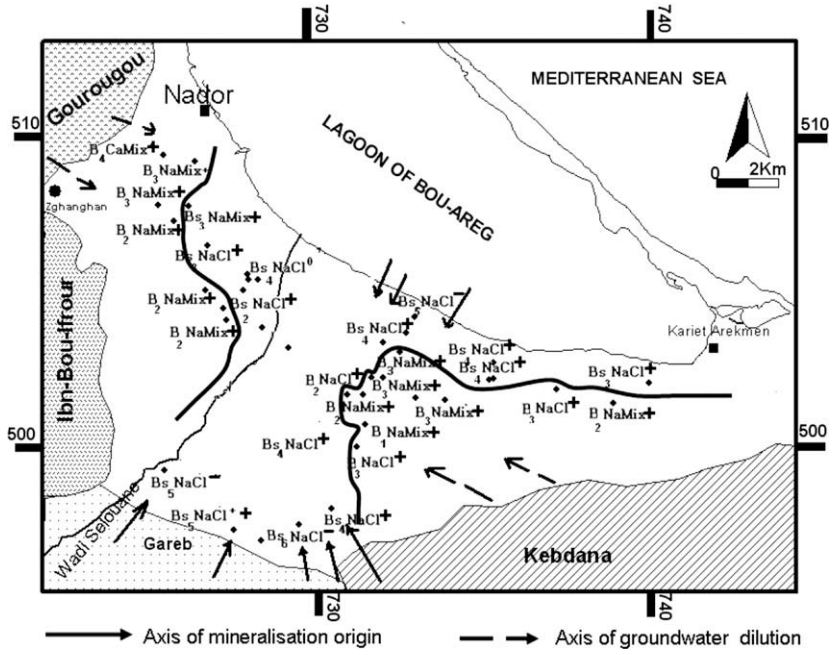

Fig. 11. Spatial distribution of the types of waters based on the Stuyfzand's classification (December 2006).

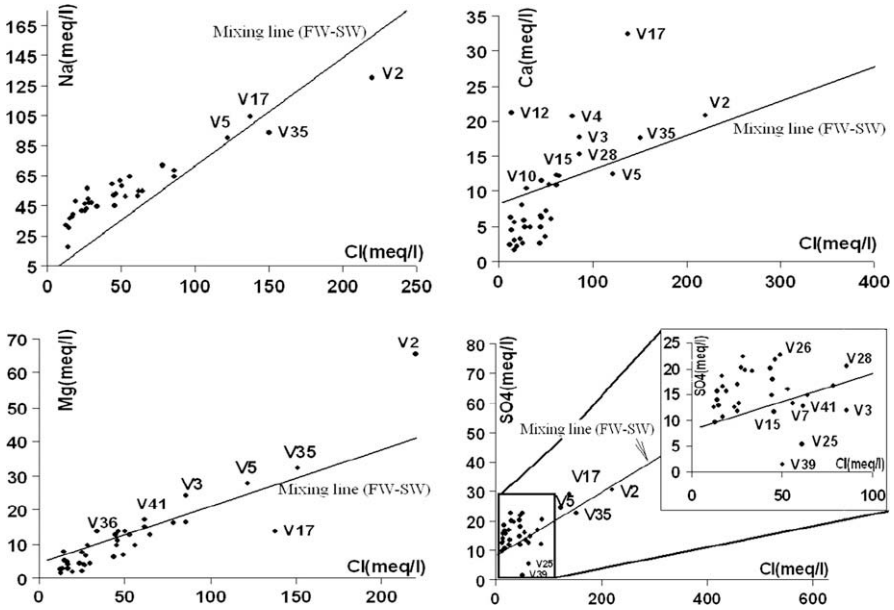

Fig. 12. Relationship between Cl content (meq/l) and 4 cations analyzed (December 2006).

these cations; the dissolution of gypsum and carbonates in the unsaturated zone is the probable factor increasing the Ca^{2+} and Mg^{2+} in groundwater. The water point (V35), located in the downstream zone of the aquifer, shows a Na^{+}/Cl^{-} ratio lower than the lagoon sample (0.72) and an increase of Ca^{2+} and Mg^{2+} concentration with respect to the mixing line (Fig. 12), which shows that the water chemistry is determined by reverse cation-exchange reactions between groundwater and the clay fraction of the aquifer material. Generally, reverse cation-exchange results during seawater intrusion, when the seawater wedge moves inland (Appelo and Postma, 1996). In this condition, the Na/Ca ratio on the surface of the exchanger in the freshwater portion of the aquifer is lower than that of the seawater front moving inland (Table 5). In addition, the water point (V2), located in the upstream zone of the aquifer, shows a Na^{+}/Cl^{-} ratio lower than the lagoon sample (0.72) and an increase of Ca^{2+} and Mg^{2+} concentration with respect to the mixing line (Fig. 12), showing that the salinization phenomenon has modified the water chemistry in this area. Water–rock interaction is thus thought to be the main factor of salinization.

The SO_4^{2-} vs Cl^{-} graph (Fig. 12) shows that some water points (located in the central and western zones) are located well above the theoretical mixing line between freshwater and saltwater. Also, (Table 4) shows that the SO_4^{2-}/Cl^{-} ratio of the majority of the samples is greater than that of the lagoon sample (0.12). The enrichment of these points with SO_4^{2-} suggests other sources, including the dissolution of gypsum and agricultural pollution (where some

Table 6
Ionic delta and saturation index of groundwater samples of Bou-Areg, December 2006.

Wells	Ionic delta					Saturation index (SI)		
	ΔNa + ΔK	ΔCa + ΔCMg	ΔHCO_3	ΔSO_4	Calcite	Dolomite	Gypsum	Halite
V2	−29.06	26.55	3.47	−1.29	0.63	1.92	−0.64	−3.42
V3	6.56	11.01	4.38	−5.44	0.61	1.50	−0.85	−4.05
V4	15.28	7.63	5.59	0.13	0.65	1.34	−0.63	−4.07
V5	1.64	1.51	4.62	3.08	0.62	1.73	−0.77	−3.80
V6	26.33	−8.84	6.68	3.06	−0.06	0.51	−1.55	−5.02
V7	24.27	−8.84	7.62	−0.85	1.06	2.46	−1.13	−4.24
V8	28.59	−4.69	9.97	6.05	0.95	2.14	−0.99	−4.71
V9	27.99	−8.44	6.98	8.62	0.52	1.37	−1.20	−4.96
V10	26.27	−4.28	6.96	8.38	1.11	1.95	−0.70	−4.64
V11	25.85	−6.48	9.48	0.71	0.66	1.31	−1.10	−4.96
V12	7.81	8.47	6.19	4.22	1.15	1.55	−0.49	−5.38
V13	10.55	−7.28	2.99	0.03	0.91	1.38	−1.00	−5.34
V14	10.94	2.85	3.90	1.93	0.73	1.75	−0.77	−4.16
V15	12.50	0.26	5.74	−1.44	0.62	1.36	−0.89	−4.47
V16	37.80	−9.24	10.07	9.02	0.96	1.93	−0.99	−4.61
V17	3.99	3.90	2.10	5.83	0.99	1.75	−0.31	−3.69
V18	25.25	−10.12	4.07	1.92	0.76	1.76	−1.29	−4.77
V19	34.48	−12.66	8.08	5.39	0.83	1.74	−1.41	−4.81
V20	30.20	−5.92	7.67	9.06	0.68	1.54	−0.93	−4.65
V21	27.25	−11.73	7.08	6.55	0.66	1.70	−1.47	−4.94
V23	24.36	−11.42	9.67	2.39	0.73	1.80	−1.38	−4.72
V24	13.36	−0.17	5.53	2.14	1.10	2.40	−0.82	−4.36
V25	7.08	0.40	4.01	−9.40	0.65	1.58	−1.27	−4.30
V26	26.39	−12.66	10.03	9.12	0.84	2.10	−1.16	−4.32
V27	24.27	−7.77	12.07	0.93	1.07	1.69	−0.96	−4.75
V28	1.97	0.71	7.38	3.03	0.78	1.73	−0.67	−4.08
V29	8.22	−1.39	7.71	−0.28	0.97	2.09	−0.83	−4.26
V30	21.05	−3.35	10.69	5.93	1.03	2.42	−1.08	−5.12
V31	19.93	−7.75	6.04	4.91	0.84	2.10	−1.08	−4.42
V33	23.78	−10.25	7.59	3.10	1.13	2.42	−1.37	−5.14
V34	27.94	−13.05	7.54	7.19	0.75	2.01	−1.31	−4.38
V35	−26.56	4.98	6.88	−1.91	0.73	1.87	−0.69	−3.75
V36	22.11	−1.32	8.06	7.83	1.04	2.66	−1.06	−4.61
V37	27.27	−4.10	9.06	11.20	1.19	2.82	−1.00	−4.67
V38	21.66	−2.55	9.14	8.61	0.82	2.11	−0.94	−4.41
V39	21.93	−2.51	9.23	−12.04	0.86	2.14	−1.95	−4.37
V40	21.47	−2.83	5.14	1.89	1.00	2.43	−1.04	−4.42
V41	10.57	3.86	5.01	−2.10	0.65	1.59	−0.91	−4.28

of these water points recorded high NO_3^- content). The SO_4^{2-}/Ca^{2+} ratio for the majority of the samples is greater than 1 (Table 5). The excess of SO_4^{2-} over Ca^{2+} reflects extra sources of SO_4^{2-} and/or a deficit of Ca^{2+}; cation exchange and calcite precipitation are suggested as the factors that remove the Ca from groundwater and decrease its content.

In order to more thoroughly determine the behavior of these cations and to identify the processes that modify the theoretical

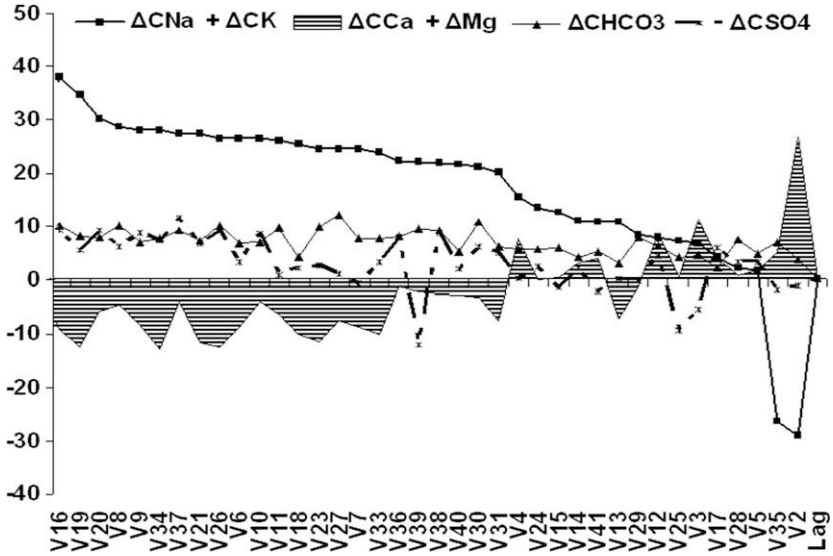

Fig. 13. Diagram of ionic delta (December 2006). L is the lagoon sample and F is the freshwater sample from the canal.

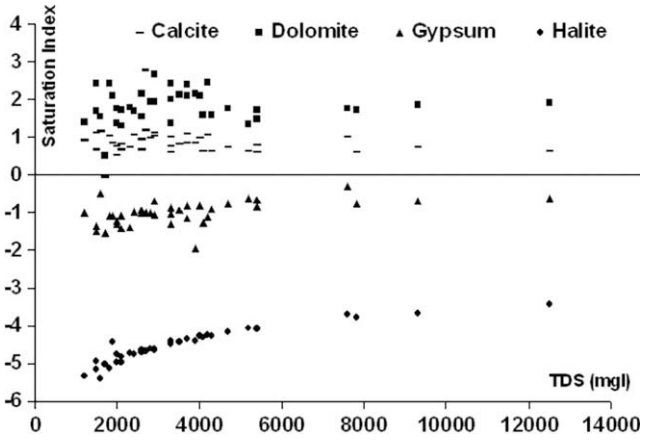

Fig. 14. Plots of Saturated Index (SI) with respect to some carbonate and evaporite minerals.

content, the ionic delta (Table 6) were calculated for each of the cations in question. Fig. 13 illustrates the various geochemical processes that occur in the groundwater. The opposite evolution of $\Delta Na^+ + \Delta K^+$ and $\Delta Ca^{2+} + \Delta Mg^{2+}$ shows that a deficit (or excess) of $Na^+ + K^+$ is compensated for by a corresponding excess (or deficit) in $Ca^{2+} + Mg^{2+}$. This could explain the different types of exchange that can occur between groundwater and the clay matrix. There is absorption of Na^+ and a release of Ca^{2+} (and Mg^{2+}) from the clay minerals in the case of salinization in samples V2 and V35, while the reverse occurs in the case of dilution (desalinization) in some aquifer samples. Cation exchangers take up Ca^{2+} from the water and release Na^+ if the Ca^{2+} concentration in the groundwater is high with respect to the concentration of Na^+ in the exchange position of clay minerals (Robertson, 1991). The similar evolution of $\Delta Na^+ + \Delta K^+$ and $\Delta Ca^{2+} + \Delta Mg^{2+}$ in some samples located in the central zone shows that the excess in these cations is due to other sources of contamination, such as the use of agricultural fertilizers. This is especially so in the case of water points V3, V4, V5, V12, V14 V17, V25 and V29 (Table 1), which have a high content of NO_3^- and/or SO_4^{2-}. (Fig. 13) shows that the ionic delta of ΔHCO_3^- is positive for all water points of aquifer and also the positive ionic delta of ΔSO_4^{2-} for the majority of the water points. This fact suggests that the dissolution of gypsum and carbonate minerals found in the aquifer deposits are the sources of these elements.

(Fig. 14) shows the plots of SI against TDS for all the investigated waters. All the groundwater samples are supersaturated with respect to calcite and dolomite (Fig. 14), suggesting that these carbonate mineral phases are present in the corresponding host rock. In fact, the presence of limestone through the aquifer deposits and the presence of calcite and dolomite detected by X-ray diffraction analysis (Bloundi, 2005; Mahjoubi et al., 2003) leads to an increase of Ca^{2+}, Mg^{2+} and HCO_3^- in the aquifer. All of the groundwater samples are undersaturated with respect to gypsum and halite (Table 6 and Fig. 14), suggesting that evaporate mineral phases are minor or absent in the host rocks. The enrichment of groundwater in Ca^{2+} as a result of both $Na^+ - Ca^{2+}$ cation exchange and dissolution of calcite in the unsaturated zone (caused by nitrification and an increase in CO_2 concentration) created favorable conditions for calcite precipitation.

4.4. Electrical tomography

(Figs. 15–17) show sections of the inverted resistivity model for L1, L2 and L3. In general, the site is characterized by a relatively low background resistivity (0.5–9 Ω/m). This variability of resistivity is observed with depth as well as laterally. The variation of lithology is quite different and each profile can be subdivided into three electrolayers, each with a specific resistivity value. Low resistivity is explained by the pores of sediments having been filled by salty water.

The resistivity profile L1 (Fig. 15) (10.1% total average RMS error) is calibrated with borehole 1021/6, taking into account the hydraulic conductivity of the water points (V35, V36, V37 and V38). The high resistivity anomaly (6.03–9.58 Ω/m) in the SW towards the inland zone corresponds well with the interpreted occurrence of gravel and minor silt. The area of very high resistivity values (>9.58 Ω/m) corresponds to coherent sediments (debris – conglomerate). Laterally and towards the NE coastline, resistivity decreases to values of 2.39–3.79 Ω/m, reflecting the transfer of salty water from the lagoon into the groundwater. These resistivity values extend 8.27–41.5 m below the surface. The lowermost electrolayer in the resistivity image has a low resistivity (0.375–0.94 / m), which is interpreted as corresponding to a clay layer, indicating that the aquifer bedrock is not far below this level.

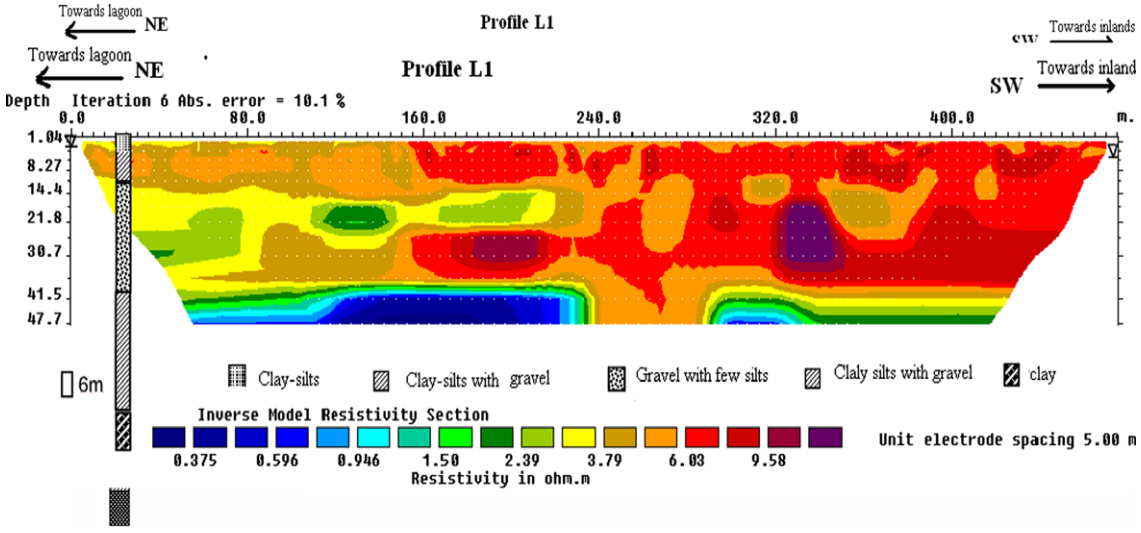

Fig. 15. Cross-section of resistivity inversion results of profile L1.

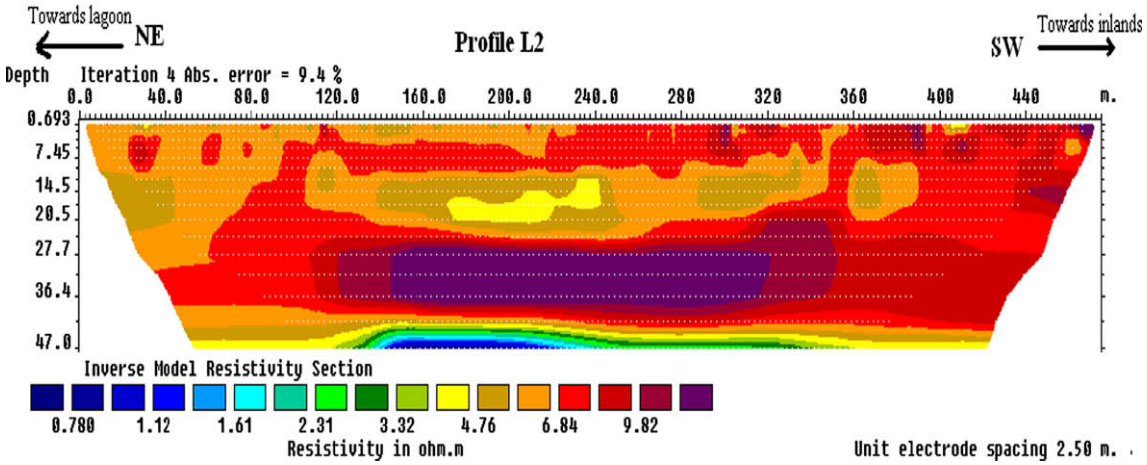

Fig. 16. Cross-section of resistivity inversion results of profile L2.

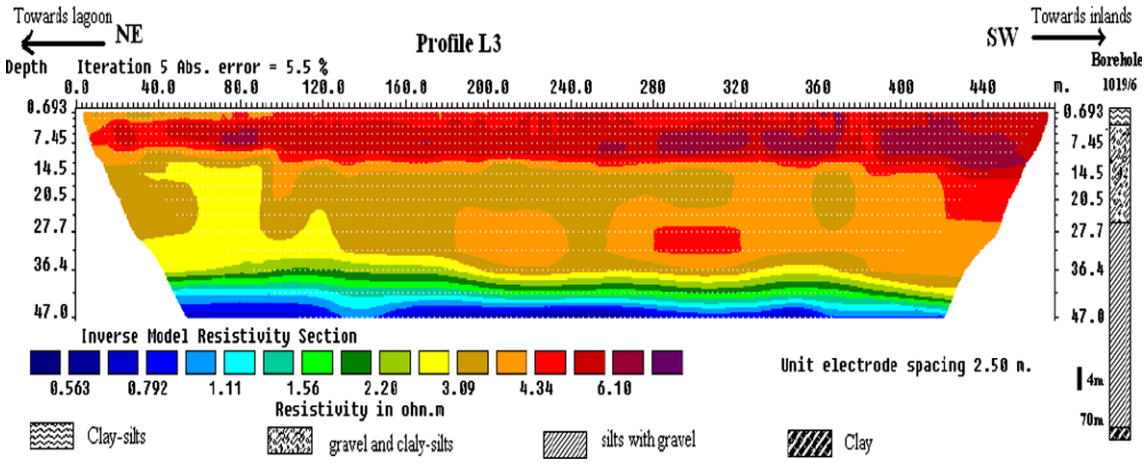

Fig. 17. Cross-section of resistivity inversion results of profile L3.

The resistivity profile L2 (Fig. 16) (9.4% total average RMS error) is a continuation of profile L1. In the NE of this section, resistivity values are low, indicating the clay layer of the bedrock, which is a continuation of the corresponding layer in profile L1. The section indicates moderate resistivity values (4.76–9.82 Ω/m), as the sediments are infiltrated by freshwater that tends to raise resistivity. The high resistivity anomaly (>9.82 Ω/m) corresponds to rigid sediments (debris – conglomerate) as in profile L1. The area of low resistivity at a depth of 14.5 m may be due to pollution by agricultural fertilizers, a conclusion supported by the observed high values of NO_3^- at V36 and V37 (Table 2).

The resistivity profile L3 (Fig. 17) (5.5% total average RMS error) is calibrated with borehole 1019/6 and with hydraulic conductivity of water points located near this profile. This section shows three distinct electrolayers. A thin layer of moderate resistivity values (4.34–6.6 Ω/m), corresponding to gravel and some silt, is visible along the top of the resistivity image and indicates the infiltration of freshwater as a result of irrigation. The pore sediments are filled by freshwater, and, consequently, the resistivity of the layer is increased. The second electrolayer comprises clayey silt with a little gravel and has low resistivity values (3.09–4.34 Ω/m). The resistivity varies laterally from the coastline inland, reflecting the incursion of seawater into the aquifer. The very low resistivity values (0.563–0.92 Ω/m) of the third electrolayer show it to be relatively impermeable.

The results of the electrical tomography surveys provide further information about the water quality of the various formations. These results also show that the zone at a depth of 8.27–41.5 m below the surface has low resistivity values, which indicates high salinity that may be due to the recent intrusion of saltwater from the lagoon into the aquifer, or to the existence of connate fossil water from ancient seawater incursion that occurred in the past (Carlier, 1964). The top layer is affected by water infiltration, which increases the resistivity. Finally, the groundwater bedrock is at a depth of 48 m.

5. Conclusions

Statistical and geochemical analyses were applied to the hydrochemical data set, and electrical tomography was used to provide insight into the regional factors and processes controlling the chemical composition and degree of salinity of groundwater in the study area.

Multivariate statistical analyses are powerful tools due to their ability to assist in making an objective interpretation. Cluster and factor analysis, applied to groundwater samples of the study area, are an effective means of manipulating, interpreting, and representing data concerning groundwater pollutants. The results of the cluster analysis showed 3 groups (A, B and C), and factor analysis showed 3 factors (F1, F2 and F3), that explained 84.09% of the total

variance in the groundwater quality. Group A and factor F1 (described as the salinization factor) included EC, Cl^-, SO_4^{2-}, Na^+, K^+ and Mg^{2+}, group B and factor F2 (the dilution processes) included Ca^{2+}, Mg^{2+}, HCO_3^- and pH, and group C and factor 3 included NO_3^- and represented agricultural and other anthropogenic sources.

The spatial distribution of the factor scores at individual wells delineated boundaries that define the areas of high salinization and pollution. Areas of high scores of factor 1 close to the coastal lagoon are due to seawater, and, at the upstream zone, the salinization is linked to the influence of marly-gypsum outcrops. High scores of factor 2 are located in the zone bounding the plain, where the recharge from the Gourougou, Ibn-Bou-Ifrour, and Kebdana massifs refreshes the groundwater and enriches the area in HCO_3^-. The anthropogenic pollutants are also detected in this study area; the high scores of factor 3 are identified in the central and eastern zones of the plain. Agricultural practices involving synthetic fertilizers have been identified as the main source of NO_3^- contamination of groundwater in the central zone, but, in the eastern zone (city of Nador), the source of NO_3^- may be linked to the leakage of domestic and industrial wastewater.

The geochemical results (Stuyfzand's method, ionic ratios and ionic deltas) showed different processes that modify the chemical composition in the Bou-Areg groundwater. Stuyfzand's method appears to be appropriate for this kind of study, and it constrains the results obtained from the statistical analysis and spatial distribution, showing two phenomena: the dilution phenomenon that occurred in the groundwater during the sampling period and the salinization phenomenon in the coastal zone by seawater intrusion and in the upstream zone caused by processes related to the dissolution of evaporite rocks from the Miocene substratum. Cation exchange also takes place and modifies the concentration of ions in the groundwater. When seawater intrudes the aquifer, Na^+ ions are released into the groundwater, and Ca^{2+} and/or Mg^{2+} are absorbed by the clay-matrix, and vice versa in the case of refreshing groundwater. The saturation index showed the precipitation and dissolution mechanism that occurred in the aquifer system. The dissolution of gypsum increased the concentrations of SO_4^{2-} and Ca^{2+}, and the dissolution of halite increased the Na^+ concentrations in the groundwater. Conversely, the Ca^{2+} and Mg^{2+} were decreased by the precipitation of calcite and dolomite.

The results of the electrical tomography surveys corroborate the geostatistical and geochemical results and provide further information about the water quality of the various formations. These results also show that the zone 8.27–41.5 m below the surface has low resistivity values, which indicates high salinity that may be due to the recent intrusion of saltwater from the lagoon into the aquifer or to the existence of connate fossil water from ancient seawater incursion that occurred in the past. The top layer is affected by water infiltration, which increases resistivity. The groundwater bedrock is close to a depth of 48 m.

This study shows that the multivariate statistical and geochemical methods and electrical tomography are excellent exploratory tools for interpreting complex water quality data and the origin of groundwater pollution. The obtained information represents a base for future hydrogeological work that will help in the planning, protection and decision-making regarding the groundwater management of the Bou-Areg plain. However, for additional corroboration of the interpretations of the origin of the salinity, isotopic analysis will be performed in the study area.

Acknowledgments

We are grateful for the support from COSTE (Oriental Center of Water Science and Technology, Oujda, Morocco), and the Moulouya Water Basin Agency. We also acknowledge Dr. I. Vadillo, from the University of Malaga, Spain, and Prof. Ph. Renard, from the University of Neuchatel, Switzerland, for their early comments about this paper. We thank Dr. A. Herczeg for handling this paper and the reviewers for their comments that improved the original paper.

Appendix A. Supplementary material

Supplementary data associated with this article can be found, in the online version, at doi:10.1016/j.apgeochem.2008.10.005.

References

Appelo, C.A.J., Postma, D., 1996. Geochemistry, Groundwater and Pollution. A.A. Balkema, USA.

Barathon, J.J., 1989. Bassins et littoraux du Rif oriental (Maroc): évolution morphoclimatique et tectonique depuis le Néogène superieur. Interuniversity Center of Mediterranean study. Ph.D., Univ. Poitiers, France.

Benson, R.H., Rakic-El Bied, K., Bonaduce, G., 1991. An important current reversal (influx) in the Rifian Corridor (Morocco) at the Tortonian-Messinian boundary: the end of the Tethys Ocean. Paleoceanog 6, 164–192.

Berthold, S., Bentley, L.R., Hayashi, M., 2004. Integrated hydrogeological and geophysical study of depressionfocused groundwater recharge in the Canadian prairies. Water Resour. Res. 40, W06505.1–W06505.14.

Bloundi, M.K., 2005. Etude geochimique de la lagune de Nador (Maroc oriental): impacts des facteurs anthropiques. Ph.D., Univ. Mohamed V. Agdal. Faculté des Sciences Rabat. Maroc.

Capaccionia, B., Diderob, M., Palettab, C., Didero, L., 2005. Saline intrusion and refreshening in a multilayer coastal aquifer in the Catania Plain (Sicily, Southern Italy): dynamics of degradation processes according to the hydrochemical characteristics of groundwaters. J. Hydrol. 307, 1–16.

Cardona, A., Carrillo-Rivera, J.J., Huizar-Alvarez, R., Graniel-Castro, E., 2004. Salinization in coastal aquifers of arid zones: an example from Santo Domingo, Baja California Sur, Mexico. Environ. Geol. 45, 350–366.

Carlier, P.H. 1964. Plaines de Gareb et Bou-Areg (Plains of Gareb and Bou-Areg). Note and Service Memory, Geology, Morocco.

Ceron, J.C., Jimenez-Espinosa, R., Pulido-Bosch, A., 2000. Numerical analysis of hydrogeochemical data: a case study (Alto Guadalentõan, southeast Spain). Appl. Geochem. 15, 1053–1067.

Cimino, A., Cosentino, C., Oieni, A., Tranchina, L., 2008. A geophysical and geochemical approach for seawater intrusion assessment in the Acquedolci coastal aquifer (Northern Sicily). Environ. Geol. 55 (7), 1473–1482.

Custodio, E., 1987. Hydrogeochemistry and tracers. In: Custodio, E. (Ed.), Groundwater Problems in Coastal Areas Studies and Reports in Hydrology, vol. 45. UNESCO, Paris, pp. 213–269.

Dakki, M., El Fallah, B., Fkhaoui, M., 2000. Diagnostic sur les zones humides (Humide zones diagnostic). MedWet Coast Project, Preliminary Report, pp. 5–15.

Diamantopoulou, P., 1999. Hydrogeological conditions of the island of Zakynthos, Ionian sea. Ph.D., Univ. Patras, Greece (in Greek).

Dörfliger, N. 2003. The state of the French Mediterranean coastal aquifers. In: López-Geta, J.A., Orden, J.A., Gómez, J.D., Ramos, G., Mejías, M., Rodríguez, L. (Eds) Coastal Aquifers Intrusion Technology: Mediterranean Countries. Publs. Inst. Geol. Min. de España. Serie: Hidrogeologia y Aguas Subterraneas No 8. Madrid, Spain, Tome II, pp. 187–206.

El Bakkali, S., 1995. Volcanologie et Magmatologie du système du Gourougou (Rif Oriental, Maroc). Ph.D., Univ. Blaise Pascal Clermont-Ferrand II, France.

El Baruni, S., 1995. Deterioration of the quality of groundwater from Suani wellfield, Tripoli, Libya. Hydrogeol. J. 3, 58–64.

El Mandour, A., Fakir, Y., Aqil, H., Boughriba, M., Zarhloule, Y., Ghomari, Y., 2008. Salinisation des eaux souterraines de la plaine de Saïdia, côte méditerranéenne orientale Maroc Centre d'hydrogéologie, Université de Neuchâtel, Edition Peter Lang. Bulletin d'Hydrogéologie 22, 43–57.

El Mandour, A., El Yaouti, F., Fakir, Y., Zarhloule, Y., Benavente, J., 2007. Evolution of groundwater salinity in the unconfined aquifer of Bou-Areg, Northeastern Mediterranean coast, Morocco. Environ. Geol. 54, 491–503.

El Mandour, A., El Yaouti, F., Fakir, Y., Zarhloule, Y., Bourhriba, M., El Haouadi, B., 2006. Origin and distribution of groundwater salinization in the unconfined coastal aquifer of Bou-Areg, Northeastern Mediterranean Coast, Morocco. Las aguas subterraneas en los paises mediterraneos. Publs. Inst. Geol. Min. de España. Serie: hidrogeologia y Aguas Subterraneas No 17. Madrid, Spain, pp. 287–294.

Eriksson, E., 1952. Composition of atmospheric precipitation; II Sulfur, chloride, iodine compounds. Tellus 4, 280–303. Bibliography.

Ferrara, V., Pappalardo, G., 2004. Intensive exploitation effects on alluvial aquifer of the Catania plain, eastern Sicily, Italy. Geofísica Internacional 43, 671–681.

Freeze, R.A., Cherry, J.A., 1979. Groundwater. Prentice Hall, Englewood Cliffs, N.J.

Gill, R.C.O., Aparicio, A., El Azzouzi, M., Hernandez, J., Thirlwall, M.F., Bourgois, J., Marriner, G.F., 2004. Depleted arc volcanism in the Alboran sea and shoshonitic volcanism in Morocco: geochemical and isotopic constraints on Neogene tectonic processes. Lithos 78, 363–388.

Grassi, S., Netti, R., 2000. Sea water intrusion and mercury pollution of some coastal aquifers in the province of Grosseto (Southern Tuscany, Italy). J. Hydrol. 237, 98–211.

Harman, H.H., 1960. Modern Factor Analysis. University of Chicago Press.
Helina, B., Pardo, R., Vega, M., Barrado, E., Fernandez, J.M., Fernandez, L., 2000. Temporal evolution of groundwater composition in an alluvial aquifer (Pisuerga River, Spain) by principal component analysis. Water Res. 34, 807–816.
Hernandez, J., Bellon, H., 1985. Chronologie K-Ar du volcanisme miocène du Rif oriental (Maroc): implications tectoniques et magmatiques. Rev. Geol. Dyn. Geog. Phys. 26, 85–94.
Hidalgo, M.C., Gruz-Sanjuhan, J., 2001. Groundwater composition, hydrochemical evolution and mass transfer in a regional detrital aquifer, Baza basin, southern Spain. Appl. Geochem. 16, 745–758.
Hsü, K.J., Ryan, W.B.F., Cita, M.B., 1973. Late Miocene desiccation of the Mediterranean. Nature 242, 240–244.
Jalali, M., 2007. Salinization of groundwater in arid and semi arid zone an example from Tajarak, Western Iran. Environ. Geol. 52, 1133–1149.
Kaiser, H.F., 1958. The varimax criteria for analytical rotation in factor analysis. Psychometrika 23, 187–200.
Kim, J.H., Yum, B.W., Kim, R.H., Koh, D.C., Cheong, T.J., Lee, J., Chang, H.W., 2003. Application of cluster analysis for the hydrogeological factors of saline groundwater in Kinjé, Korea. Geosci. J. 7, 313–322.
Krijgsman, W., Langereis, C.G., Zachariasse, W.J., Boccaletti, M., Moratti, G., Gelati, R., Iaccarino, S., Papani, G., Villa, G., 1999. Late Neogene evolution of the Taza-Guercif basin (Riftian Corridor, Morocco) and implications for the Messinian salinity crisis. Mar. Geol. 153, 147–160.
Lambrakis, N.J., Voudouris, K.S., Tiniakos, L.N., Kallergis, G., 1997. Impact of simultaneous action of drought and overpumping on quaternary aquifers of Glafkos basin (Patras region, western Greece). Environ. Geol. 29, 209–215.
Lashkaripour, G.R., Nakhaei, M., 2005. Geoelectrical investigation for the assessment of groundwater conditions: a case study. Annals Geophys. 48, 937–944.
Lee, S.H., Kim, K.G., Ko, I., Lee, S.G., Hwang, H.S., 2001. Geochemical and geophysical monitoring of saline water intrusion in Korean paddy fields. Environ. Geochem. Health 24, 277–291.
Liu, C.W., Lin, K.H., Kuo, Y.M., 2003. Application of factor analysis in the assessment of groundwater quality in a blackfoot disease area in Taiwan. Sci. Total Environ. 313, 77–89.
Loke, M.H., 2002. Rapid 3D resistivity and IP inversion using the least-squares method. Geoelectrical imaging 2D & 3D, Geotomo software.
Loke, M.H., Barker, R.D., 1996. Practical techniques for 3D resistivity surveys and data inversion. Geophys. Prospect. 44, 499–523.
Lourens, L.J., Hilgen, F.J., Zachariasse, W.J., Van Hoof, A.A.M., Antonrakou, A., Vergnaud-Grazzini, C., 1996. Evaluation of the Pliocene to early Pleistocene astronomical timescale. Paleoceanog 11, 391–413.
Löwner, M.O., Preston, N.J., Dikau, R., 2005. Reconstruction of a colluvial body using geoelectrical resistivity. Z. Geomorph. N. F. 49, 225–238.
Mahjoubi, R., Kamel, S., El Moumni, B., Noack, Y., Parron, C., 2003. Nature, origine et répartition de la phase argileuse de la lagune de Nador (Maroc Nord Oriental). Geologica Belgica 6, 31–42.
Morel, J.L., 1985. Les événements tectoniques et volcaniques responsable de la régression messinienne dans le Maroc septentrional: exemple du bassin d'Iddouyine (Segangane – Rif oriental – Maroc). Inst. Sci. Bull. 9, 97–106.
Morel, J.L., 1989. Evolution paléogéographique et tectonique du rif (Maroc) du Tortonien à l'actuel. C. R. Acad. Sci. Paris 309, 2053–2059.
Petalas, C.P., Diamantis, I.B., 1999. Origin and distribution of saline groundwaters in the upper Miocene aquifer system, coastal Rhodope area, Northeastern Greece. Hydrogeol. J. 7, 305–316.
Reeve, A.S., Siegel, D.I., Glaser, P.H., 1996. Geostatistical analysis of peat pore-water chemistry: Hudson Bay Lowlands, Ontario, Canada. J. Hydrol. 181, 285–304.
Robertson, F.N. 1991. Geochemistry of groundwater in alluvial basins of Arizona and adjacent parts of Nevada, New Mexico and California. U. S.Geol. Surv. Prof. Paper 1406–C.
Stamatis, G., Voudouris, K., 2003. Marine and human activity influences on the groundwater quality of southern Korinthos area (Greece). Hydrol. Process. 17, 2327–2345.
Stumm, W., Morgan, J.J., 1996. Aquatic chemistry—chemical equilibria and rates in natural waters. John Wiley and Sons, New York, USA.
Stuyfzand, P.J., 1986. A new hydrochemical classification of water types: principles and application to the coastal dunes aquifer system of the Netherlands. SWIM 9th Delft.
Tsourlos, P.I., Ogilvy, R.D., 1999. An algorithm for the 3D inversion of tomographic resistivity and induced polarization data: preliminary results. J. Balkan Geophys. Soc. 2 (2), 30–45.
Vincenzo, F., Giovanna, P., 2003. Salinization of coastal aquifers in the southwestern hyblean plateau (SE Sicily, Italy). In: López-Geta, J.A., Orden, J.A., Gómez, J.D., Ramos, G., Mejías, M., Rodríguez, L., (Eds.), Publs. Inst. Geol. Min. de España. Serie: Hidrogeologia y Aguas Subterraneas No 8. Madrid, Spain, Tome I, pp. 103–112.
Word, J.H., 1963. Hierarchical grouping to optimize an objective function. J. Am. Stat. Assoc. 58, 236–244.
Worden, R.H., Manning, D.A.C., Bottrell, S.H., 2006. Multiple generations of high salinity formation water in the Triassic Sherwood Sandstone: Wytch Farm oilfield, onshore UK. Appl. Geochem. 21, 455–475.
Zhang, J., Mackie, R.L., Madden, T.R., 1995. 3D resistivity forward modeling and inversion using conjugate gradients. Geophysics 60, 1313–1325.